Chemistry–A European Journal
Research Article
doi.org/10.1002/chem.202301760
Chemistry Europe
European Chemical Societies Publishing
www.chemeurj.org

Acidic Properties of Known and New COOH-Functionalized M(IV) Metal-Organic Frameworks

Mirjam Patricia Margarete Poschmann,[a] Karl Petter Lillerud,[b] and Norbert Stock*[a]

Abstract: Herein, we report two new COOH-functionalized metal-organic frameworks (MOFs) of composition $[M_6O_4(OH)_6(PMA)_2(H_2PMA)]\times H_2O$, M=Zr, Hf), denoted CAU-61, synthesized by using pyromellitic acid (H_4PMA), a tetracarboxylic acid, as the linker and acetic acid as the solvent. The structure was determined from powder X-ray diffraction data and one-dimensional inorganic building units are connected through tetracarboxylate as well as dicarboxylate linker molecules, resulting in highly stable microporous framework structures with limiting and maximum pore diameter of ~3.6 and ~5.0 Å, respectively, lined with –COOH groups. Thermal stabilities of up to 400 °C in air, chemical stability in water at pH 1 to 12 and water uptake of 17 mol/mol prompted us to study the proton exchange of the μ_2-OH, μ_3-OH of the IBU and –COOH groups of the linker by titration with LiOH. Comparison of the pK_a values with three UiO-66 derivatives confirms distinct pK_a value ranges and trends for the different acidic protons. Furthermore, the preparation of Zr–CAU-61 membranes and first results on permeation of dyes and ions in aqueous solutions are presented.

Introduction

Metal-organic-Frameworks (MOFs) are of high interest because of their modular assembly and therefore tunable pore sizes and structures. The high thermal, chemical and mechanical stability of most Zr-based MOFs and the comparatively high occurrence of zirconium make these compounds particularly promising for various practical applications.[1–3] The first carboxylate-based Zr-MOF, UiO-66[4] (UiO=Universitetet i Oslo), exhibits one of the most common and therefore well characterized structure types in Zr-MOF chemistry. By varying the linker molecules, an easy functionalization of the pore surface is possible and generates the UiO-66 type family. Representatives are discussed for example for CO_2 capture,[5] as acidic catalysts[6,7] and as membrane materials,[8–10] and the synthesis and properties of acidic MOFs have been recently reviewed.[11] MOFs as acidic catalysts are of special interest as the pores can favor the formation of a particular isomer or provide active sites in direct proximity.[12,13] Membrane materials are important for example for gas separation,[14] water purification[15,16] or separation of organic solvents.[17] Membranes containing MOFs are often MOF films grown on a porous substrate or mixed matrix membranes with micro- or nanoparticles as fillers in polymer matrices.[15,18,19]

Most Zr-MOFs contain the hexanuclear cluster $\{Zr_6O_4(OH)_4\}$ as the inorganic building unit (IBU) although they can assemble into various topologies as observed for example in DUT-67[20] (DUT = Dresden University of Technology), MOF-808[21] and PCN-222[22] (PCN = porous coordination network). In addition, some Zr-MOFs with other IBUs are known, for example CAU-22,[23] CAU-27,[24] CAU-39[25] Zr_{12}–TPDC[26] ($TPDC^{2-}$ = triphenyldicarboxylate) CAU-45[27]/MIP-206[28] (CAU = Christian-Albrechts Universität; MIP = material of the Institute of Porous Materials of Paris) and MIL-140[29] (MIL = Matériaux de l'Institut Lavoisier). In the first examples, different kinds of condensed hexanuclear clusters and in MIL-140 a chain of $\{ZrO_7\}$ polyhedra were observed. These IBUs were found when non-standard linker molecules, solvents or reaction conditions were employed, such as monocarboxylic acids as solvents or harsh synthesis conditions. High-throughput (HT) methods allow a fast, efficient and systematic screening of chemical and process parameters thus facilitating the discovery of new compounds and are therefore the ideal tool to screen reaction conditions.

Herein, we report on the synthesis and characterization of CAU-61, which was discovered in a HT linker screening experiment, its acidic properties in comparison to three other acidic UiO-66 derivatives, and the preparation of free standing membranes that were used in permeation experiments in aqueous solutions.

[a] M. P. M. Poschmann, Prof. Dr. N. Stock
Department of Inorganic Chemistry
Christian-Albrechts-University
Max-Eyth-Straße 2, 24118 Kiel (Germany)
E-mail: stock@ac.uni-kiel.de

[b] Prof. Dr. K. P. Lillerud
Department of Chemistry
University of Oslo
Blindern, 0315 Oslo (Norway)

Supporting information for this article is available on the WWW under https://doi.org/10.1002/chem.202301760

Results and Discussion

The discovery and synthesis optimization of M–CAU-61 was performed using our high throughput setup with 2 mL Teflon inserts.[30] Based on the results of a previous study,[27] acetic acid was employed as the solvent and reaction temperatures of 180 °C were used. Eight linker molecules with different geometry, number of –COOH groups and size were chosen and the influence of NaOH and HCl as modulators on the phase formation and the crystallinity was determined. The use of pyromellitic acid (H_4PMA) resulted in crystalline products. An excess of $ZrCl_4$ ($ZrCl_4$:linker = 1:0.5) leads to the formation of CAU-61, while with increasing amounts of linker, mixtures of CAU-61 and UiO-66 are observed.

Synthesis optimization resulted in the optimized composition of the reaction mixture of composition $ZrCl_4:H_4PMA:HCl:H_2O:CH_3COOH = 1:0.5:1:3.4:144$ and $HfCl_4:H_4PMA:HCl:H_2O:CH_3COOH = 1:0.5:2:6.9:143$ which led after a reaction time of 70 h at 180 °C to a microcrystalline reaction product of CAU-61. Details on the syntheses are given in Supporting Information section 2.

For structure elucidation, a PXRD pattern of Zr–CAU-61 and the program TOPAS[31] were used to perform indexing and Pawley refinement. Unit cell parameters indicated structural similarities to CAU-22 and therefore, a structural model was built using Materials Studio.[32] However, the successful Rietveld refinement against PXRD data using TOPAS[31] was only possible by removing monocarboxylate ligands from the starting model and changing the framework connectivity. Details of the structure determination are given in the Supporting Information section 3. The same IBU as previously observed for CAU-22 is found, which consists of edge sharing hexanuclear clusters that form chains (Table S3.1, Figure 1a). Thus, there are acidic μ_3-OH in the hexanuclear cluster and μ_2-OH groups from cluster condensation present. In contrast to CAU-22, a new connectivity by the linker molecules is found. According to the composition $[M_6O_4(\mu_3\text{-OH})_4(\mu_2\text{-OH})_2(PMA)_2(H_2PMA)]$, two linker molecules per formula unit coordinate with four and the third linker with two carboxylate groups (Figure 1c). The non-coordinating –COOH groups are accessible through the one-dimensional, triangular pores (Figure 1b). The limiting and maximum pore diameters were determined to be ~3.6 Å and ~5.0 Å, respectively. Due to the different framework connectivity, the topology changes from the uninodal net **bnn** (point symbol $\{4^6.6^2\}$) for CAU-22 to a three nodal 3,5,6-c net (point symbol $\{3^2.4^6.5^2.6^3.7.8\}_4\{3^4.4^2.8^4\}\{4^2.6\}_4$) in CAU-61 (Figure 1d and Supporting Information section S3).

To further confirm the plausibility of the refined structure, a geometry optimization was performed in Materials Studio[32] in space group P-1 using the code Dmol3. Only very small differences between the calculated and the refined structure were found (further details in Supporting Information section S4). The refinement of the Hf–CAU-61 was successfully performed using the structure of Zr–CAU-61.[33] The composition of the two compounds was confirmed by

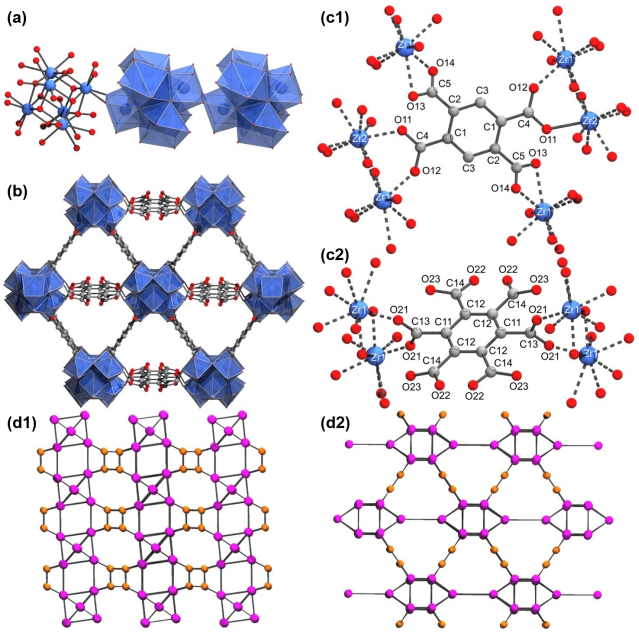

Figure 1. Top: IBU (a) and structure of M–CAU-61 (with M=Zr, Hf) viewed along the one-dimensional pores (b) and the two linker molecules with different coordination geometry (c1, c2). Bottom: Topology of M–CAU-61 in *b*- (d1) and *c*-direction (d2). Nodes representing the carboxylate groups are colored in pink and those representing the linker molecules in orange.

thermogravimetric (Tables S8.1 and S8.2) and elemental analysis (Table S7.1) as well as ^{1}H NMR (Figures S6.1 and S6.2).

The thermal properties were investigated by thermogravimetric analysis (TGA), temperature programmed desorption / mass spectrometry (TPD/MS) and variable temperature powder X-ray diffraction (VT-PXRD). TGA demonstrates thermal stabilities of 390 °C for Zr– and Hf–CAU-61. The weight losses prior to framework decomposition are due to the loss of adsorbed water molecules and water molecules resulting from the dehydration of the IBU (Figure S8.2). VT-PXRD measurements demonstrate structural integrity up to the decomposition temperature (Supporting Information section 8). Above 400 °C, a slight shift of reflection positions and a steady loss of intensity up to total decomposition at 470 °C (for Zr–CAU-61) and 480 °C (for Hf–CAU-61) are observed.

Sorption measurements using nitrogen (at 77 K), water and carbon dioxide (at 298 K) confirm the microporosity of CAU-61 (Supporting Information, section S9). With N_2 as the adsorptive, type 1 isotherms are observed and specific surface areas of $a_{BET} = 320$ and 285 m^2/g were calculated for Zr– and Hf–CAU-61, respectively. The isotherm shape and the a_{BET} value were also determined for Zr–CAU-61 using the Sorption Module as implemented in Materials Studio[32] and are in good agreement ($a_{BET,\,calc.} = 308$ m^2/g). CAU-61 is hydrophilic with a maximum uptake of 17 mol water per mol MOF, but adsorbs 3.5 and 4 mol/mol CO_2, respectively. Details are given in the Supporting Information section S9.

CAU-61 is stable in several organic solvents, water, aqueous HCl- and NaOH-solutions in a pH range of 1 to 12 and phosphate buffer solution. At pH = 13 the structure

decomposes and an X-ray amorphous product is formed (Supporting Information section S11).

The stability in aqueous solutions and the presence of accessible μ_2-OH, μ_3-OH and –COOH groups at the IBU and the linker, respectively, prompted us to study and compare the acidic properties to three known and well-studied UiO-66 type materials, i.e. UiO-66-BDC, UiO-66-TMA and UiO-66-PMA (Figure 2, top, H_2BDC = benezenedicarboxylic acid, H_3TMA = trimellitic acid, H_4PMA = pyromellitic acid). These compounds exhibit additional acidic groups, i.e. coordinating H_2O molecules and OH^- ions, due to the presence of linker defects. The amount of linker defects for each sample was additionally determined by TGA measurements (Table S13.2). Details on syntheses and characterization of the UiO-66 type compounds are given in the Supporting Information section S12.

Sample preparation prior to titration experiments is a very important aspect to obtain reproducible results. All samples must be stirred multiple times in water to remove all impurities and the pH of the starting solution must be adjusted by adding HCl in order to be able to determine the first pK_a value. Titrations with LiOH solution were performed using a procedure similar to that described by Klet et al.[34] In general, ~50 mg MOF were dispersed in 60 mL water, pH was adjusted to 2.8 by addition of diluted HCl and the titrations were carried out with LiOH solutions (c. = 0.01 to 0.05 mol/L) and titration rates between 0.1 and 0.5 mL/min, depending on the MOF. This is described in detail in Supporting Information S13.1.

The titration curves of all five samples are given in the Supporting Information S13, here the ones for Zr–UiO-66-BDC and Zr–CAU-61 are presented (Figure 2, bottom).

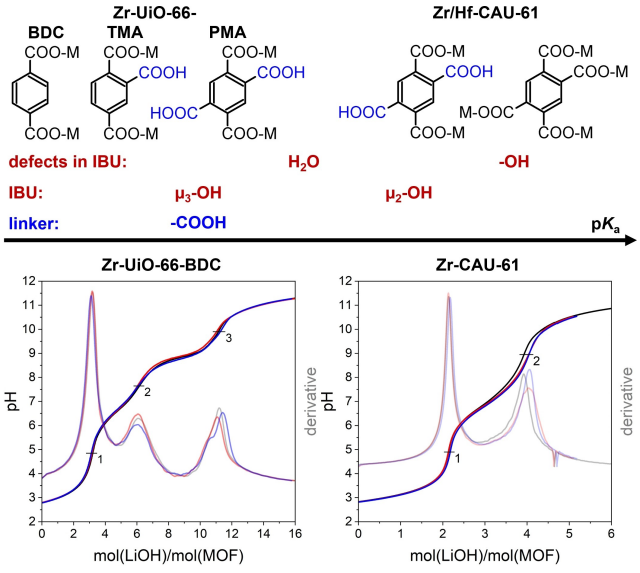

Figure 2. Top: Acidic groups in the linker molecules (blue) and the IBU (red) in the UiO-66 type MOFs and in Zr/Hf–CAU-61 and their approximate order of pK_a values. Bottom: Titration curves of Zr–UiO-66-BDC (left) and Zr–CAU-61 (right) with the three and two marked equivalent points (EPs), respectively.

In the titration curve of Zr–UiO-66-BDC three different equivalent points (EP) are observed (Figure 2, bottom left, and Supporting Information section S13.2). The first EP can be attributed to the μ_3-OH groups in the cluster, and the second and third EP are assigned to the H_2O and OH^- ligands, respectively.[34] The pK_a values differ slightly from those reported earlier (Table S13.3).[34] This can be explained by the different sample preparation, the defect rich structure or the slightly different titration procedure (Supporting Information section S13.1).

The influence of non-coordinating –COOH groups in the framework on the titration curves was systematically studied for the other compounds. The deprotonation of the acidic protons of μ_3-OH and –COOH groups occurs in a similar pH range. Therefore, only an average pK_a value can be given (Figure 3). Titration curves of Zr–UiO-66-TMA and Zr–UiO-66-PMA (Supporting Information sections S13.3 and S13.4) are very similar. The pK_a values of the three UiO-66 type MOFs are listed in Figure 3. Similar pK_a values for the deprotonation of the μ_3-OH and –COOH groups are found, but the pK_a values associated with the linker defects ($5.98 < pK_a < 6.52$ and $8.35 < pK_a < 8.81$) shift to smaller values the more carboxylate groups are in the linker molecule. This is due to the -I effect of the –COOH groups, which causes a slight decrease of the partial charges of the Zr^{4+} ions, which in turn increases the acidity of the coordinating –OH and H_2O groups. This observation is in agreement with the results of Ragon et al. who investigated the Lewis and Brønsted acidity of Zr–UiO-66-BDC, Zr–UiO-66-TMA and Zr–UiO-66-PMA by IR and acetonitrile sorption experiments.[35] The results of the titration experiments, i.e. the difference between the EP1 and EP3 values, can be used to determine the number of linker defects (see Supporting Information 13.1). Thus for UiO-66-BDC, -TMA and -PMA, defect concentrations of 1.25, 1.5 and 1.5 linker molecules per formula unit were found (Tables S13.2–S13.4). These values are in agreement with the results of the TG analyses.

Zr–CAU-61 and Hf–CAU-61 are almost defect-free according to the TG analysis and accordingly only two EP values are observed in the titration curves (Figure 2 and Supporting Information sections S13.5 and S13.6). The pK_a values can be assigned to the μ_3-OH/–COOH and the μ_2-OH groups respectively. The values of Hf–CAU-61 are slightly lower than those of the Zr analog (3.09/3.16 and 6.83/6.94, respectively) which is consistent with the results described for UiO-66-BDC

	μ_3-OH / -COOH	H_2O	μ_2-OH	-OH	pK_a
Zr-UiO-66:	3.15	6.52		8.81	
Zr-UiO-66-TMA:	3.11	6.03		8.56	
Zr-UiO-66-PMA:	3.18	5.98		8.35	
Zr-CAU-61:	3.16		6.94		
Hf-CAU-61:	3.09		6.83		

Figure 3. Assignments of the pK_a values determined by titrations of Zr–UiO-66-BDC, Zr–UiO-66-TMA, Zr–UiO-66-PMA, Zr–CAU-61 and Hf–CAU-61 with LiOH solution.

compounds.[34] The acidity of the μ_2-OH groups is between that of the μ_3-OH and the OH– ligands.

Thus, titration is a powerful instrument to investigate the acidity of different acidic groups in a MOF.

As the narrow pores of M–CAU-61 are accessible to metal ions and the compounds are highly stable in water, free standing MOF-membranes were prepared and tested in osmosis cells (details in Supporting Information section S14) with Patent Blue V and metal chlorides of Li^+, Na^+, K^+, Mg^{2+} and Ca^{2+}. Pure MOF membranes of 0.6 mm thickness and 2 cm in diameter proofed to be mechanically and chemically stable. Chemical stability was confirmed by PXRD (section S14.11). Diffusion of water molecules through the pure MOF membrane is clearly seen (Figures 4, and S14.1). Ion transport was first detected by conductivity and pH measurements (Figure S14.9), and the metal ion concentrations were recorded by ICP-OES. Metal ions diffuse slowly through the membrane, but no size-dependent sieving effect was found (Table S14.2). This is probably due to interparticle diffusion and therefore the use of the binder SilRes MP50E®, up to 15 wt.%, was tested. Patent Blue V was chosen as a large, colored analyte. Increasing the amount of binder leads to a decrease of permeation as determined visually by the color changes (Figure 4, left, Figures S14.1–S14.8). For a membrane containing 15 wt.% of the binder, no color change was observed after one week. Subsequently, membranes containing 5 and 10% binder were used in a permeation study employing a solution containing all five metal salts at concentrations of approximately 0.25 mol/L. The results are presented in Figure 4, right and in Tables S14.3–S14.4, Figure S14.9–14.13. As the binder content increases, the permeation flux decreases. Although diffusion of all ions through the membrane is observed, the permeation flux of K^+ ions is higher compared to the other ions (Figures S14.11 and S14.13). This can be explained by the smaller Stokes radius of the K^+ ion (Table S14.1). There is plenty of room for optimizing the permeation properties of such membranes, such as the use of other binder, the thickness and density of the membrane, but these studies are not within the scope of this study.

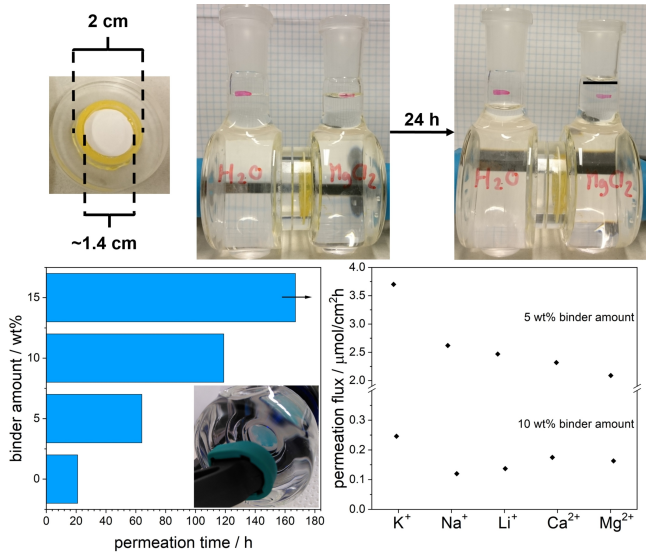

Figure 4. Top: Image of the MOF membrane with grease, which was used for sealing and volume change in osmosis cell with $MgCl_2$ solution (1 mol/L). Bottom: Visually determined permeation time for Patent Blue V depending on the binder amount (left) and calculated permeation flux for the ions K^+, Na^+, Li^+, Ca^{2+} and Mg^{2+} for membranes with 5 and 10 wt.% binder SilRes MP50E® (right). No permeation of Patent Blue V in a membrane containing 15 wt.% was detected after 1 week (indicated by the arrow).

Conclusions

In conclusion, we presented the discovery, synthesis optimization and crystal structure of a new, highly stable MOF denoted as M–CAU-61 (M=Zr, Hf). It contains a rarely observed IBU and the framework exhibits small pores and non-coordinating –COOH groups. The acidic properties were determined by titration experiments and compared with other Zr-MOFs. In contrast to the other Zr-MOFs investigated in this study, CAU-61 contains negligible amounts of linker defects. The high chemical and mechanical stability prompted us to test free standing and binder containing membranes using Zr–CAU-61. Osmosis through the membranes was observed and for a mixture of Li^+, Na^+, K^+, Mg^{2+} and Ca^{2+} ions the highest permeation flux was found for K^+.

Supporting Information

The authors have cited additional references within the Supporting Information.[36–43]

Experimental Section

All chemicals were used as received without further purification.

Synthesis of Zr–CAU-61: 420 mg $ZrCl_4$ (1.8 mmol) and 229 mg H_4PMA (0.9 mmol) were transferred to a 30 mL Teflon insert. 14.85 mL acetic acid and 150 µL HCl (1.8 mmol) were added. The sealed reactor was heated at 180 °C for 70 h and cooled to RT within 10 h. The colorless powder was isolated by filtration and washed with 30 mL water and 30 mL acetone. (EA: meas. [calc.] C = 21.0[21.0] H = 2.5[2.5] wt%; NMR: 500 mHz, sample dissolved in 20% NaOD in D_2O: 6.92 (linker), 4.90 (D_2O), 2.64 (acetone), 1.29 (acetic acid) ppm; yield: 409 mg (~26%).

Synthesis of Hf–CAU-61: 577 mg $HfCl_4$ (1.8 mmol) and 229 mg H_4PMA (0.9 mmol) were transferred to a 30 mL Teflon insert. 14.70 mL acetic acid and 300 µL HCl (3.6 mmol) were added. The sealed reactor was heated at 180 °C for 70 h and cooled to RT within 10 h. The colorless powder was isolated by filtration and washed with 30 mL water and 30 mL acetone. (EA: meas. [calc.] C = 16.2[15.5] H = 2.0[2.3] wt%; NMR: 500 mHz, sample dissolved in 20% NaOD in D_2O: 6.92 (linker), 4.90 (D_2O), 2.64 (acetone) 1.30 (acetic acid) ppm; yield: 702 mg (~34%).

Characterisation: Initial PXRD measurements were performed using a Stoe Stadi P diffractometer equipped with an xy-stage and a Mythen 1 K detector operating with Cu $K_{\alpha 1}$ radiation. PXRD measurements for the structure determination were carried out

with a Stoe Stadi MP diffractometer in transmission geometry using Cu $K_{\alpha1}$ radiation. VT-PXRD measurements were performed using a Stoe Stadi P diffractometer equipped with a STOE capillary furnace and a Mythen 1 K detector operating with Cu $K_{\alpha1}$ radiation. IR spectra were measured on a Bruker ALPHA-P A220/D-01 FTIR spectrometer equipped with an ATR unit. DTA/TG data were recorded using a Linseis STA 1600 analyzer with heating rates of 4 or 8 K/min under floating air. The TPD-MS measurement was performed using a home-build setup for the oven with a heating rate of 4 °C/min, synthetic air (N_2/O_2) and a Pfeiffer Vacuum Omnistar online mass spectrometer with MID for gas detection. Elemental analyses were carried out using a EuroVector EuroEA analyzer. NMR spectra were recorded with a Bruker DRX 500 spectrometer and the MOFs were dissolved in 20 % NaOD in D_2O. Nitrogen and water sorption measurements were performed with a BELSORP-max instruments (BEL Japan Inc.) at −196 °C (77 K) and 25 °C, respectively. CO_2 sorption measurements were carried out using a BESLORP-miniX apparatus (Microtrac) at 25 °C. ICP-OES measurements were performed with an ICP-OES Avio 200 instrument (Perkin Elmer). Particle size and charge were determined using a DelsaNano C Submicron Particle Size Analyzer equipped with 3 mL cuvettes or the zeta potential cell. Osmosis cells were built using two glass cells with a maximum volume of 40 mL each and a membrane bracket for membranes with a diameter of 2 cm. pH measurements were performed with an iUnitrode (Metrohm) and conductivity measurements with a Greisinger GMH 3451. Titration curves were recorded using a pH module of Metrohm equipped with a Dosino and an iUnitrode. For each titration ~50 mg of MOF was dispersed in ~60 mL of water by stirring and 1 min treatment in an ultrasonic bath. All samples were titrated at least three times with and without additional HCl. The LiOH solution was always prepared fresh or used within one week of preparation. The concentration of the LiOH solution was determined by titration of oxalic acid dihydrate. Sample pretreatment, preparation and titration rate were chosen individually and more details are given in Supporting Information Table S1.1 and section S13.

Acknowledgements

Financial support by the state of Schleswig-Holstein is acknowledged. The authors thank Bastian Achenbach, Felix Steinke, Niklas Ruser, Sebastian Mangelsen, Melina Ottenberg and the spectroscopic section of the department of inorganic chemistry (University of Kiel) and Tomas C. Lanzac, Chris W. Affolter, Hanne Martinsen (University of Oslo) for their support and for various measurements. We thank Erik Svensson Grape for the topological analysis of the structure. Open Access funding enabled and organized by Projekt DEAL.

Conflict of Interests

The authors declare no conflict of interest.

Data Availability Statement

The data that support the findings of this study are available in the supplementary material of this article.

Keywords: acidity · LiOH titration · metal-organic framework · osmosis · zirconium

[1] Y. Bai, Y. Dou, L.-H. Xie, W. Rutledge, J.-R. Li, H.-C. Zhou, *Chem. Soc. Rev.* **2016**, *45*, 2327–2367.
[2] L. Feng, J. Pang, P. She, J.-L. Li, J.-S. Qin, D.-Y. Du, H.-C. Zhou, *Adv. Mater.* **2020**, *32*, 2004414.
[3] M. Rimoldi, A. J. Howarth, M. R. DeStefano, L. Lin, S. Goswami, P. Li, J. T. Hupp, O. K. Farha, *ACS Catal.* **2017**, *7*, 997–1014.
[4] J. H. Cavka, S. Jakobsen, U. Olsbye, N. Guillou, C. Lamberti, S. Bordiga, K. P. Lillerud, *J. Am. Chem. Soc.* **2008**, *130*, 13850–13851.
[5] A. D. Wiersum, E. Soubeyrand-Lenoir, Q. Yang, B. Moulin, V. Guillerm, M. B. Yahia, S. Bourrelly, A. Vimont, S. Miller, C. Vagner, M. Daturi, G. Clet, C. Serre, G. Maurin, P. L. Llewellyn, *Chem. Asian J.* **2011**, *6*, 3270–3280.
[6] A. Rapeyko, M. Rodenas, F. X. Llabrés i Xamena, *Adv. Sustainable Syst.* **2022**, *6*, 2100451.
[7] P. Lu, H. Li, M. Li, J. Chen, C. Ye, H. Wang, T. Qiu, *Fuel* **2022**, *324*, 124537.
[8] X. Wang, Q. Lyu, T. Tong, K. Sun, L.-C. Lin, C. Y. Tang, F. Yang, M. D. Guiver, X. Quan, Y. Dong, *Nat. Commun.* **2022**, *13*, 266.
[9] J. Hou, H. Wang, H. Zhang, *Ind. Eng. Chem. Res.* **2020**, *59*, 12907–12923.
[10] R. M. Rego, M. D. Kurkuri, M. Kigga, *Chemosphere* **2022**, *302*, 134845.
[11] B. N. Bhadra, I. Ahmed, H. J. Lee, S. H. Jhung, *Coord. Chem. Rev.* **2022**, *450*, 214237.
[12] M. Yoon, R. Srirambalaji, K. Kim, *Chem. Rev.* **2012**, *112*, 1196–1231.
[13] L.-L. Ling, W. Yang, P. Yan, M. Wang, H.-L. Jiang, *Angew. Chem. Int. Ed.* **2022**, *61*, e202116396.
[14] D. De Meis, M. Richetta, E. Serra, *Interceram* **2018**, *67*, 16–21.
[15] T. Le, X. Chen, H. Dong, W. Tarpeh, A. Perea-Cachero, J. Coronas, S. M. Martin, M. Mohammad, A. Razmjou, A. R. Esfahani, N. Koutahzadeh, P. Cheng, P. R. Kidambi, M. R. Esfahani, *Ind. Eng. Chem. Res.* **2021**, *60*, 6869–6907.
[16] H. Wei, S. Zhao, X. Zhang, B. Wen, Z. Su, *Mater. Today Energy* **2021**, *22*, 100856.
[17] S. Liu, G. Zhou, G. Cheng, X. Wang, G. Liu, W. Jin, *Sep. Purif. Technol.* **2022**, *299*, 121729.
[18] B.-M. Jun, Y. A. J. Al-Hamadani, A. Son, C. M. Park, M. Jang, A. Jang, N. C. Kim, Y. Yoon, *Sep. Purif. Technol.* **2020**, *247*, 116947.
[19] C. J. Davey, D. Leak, D. A. Patterson, *Membranes* **2016**, *6*, 17.
[20] V. Bon, I. Senkovska, I. A. Baburin, S. Kaskel, *Cryst. Growth Des.* **2013**, *13*, 1231–1237.
[21] H. Furukawa, F. Gándara, Y.-B. Zhang, J. Jiang, W. L. Queen, M. R. Hudson, O. M. Yaghi, *J. Am. Chem. Soc.* **2014**, *136*, 4369–4381.
[22] D. Feng, Z.-Y. Gu, J.-R. Li, H.-L. Jiang, Z. Wei, H.-C. Zhou, *Angew. Chem. Int. Ed.* **2012**, *51*, 10307–10310.
[23] S. Waitschat, H. Reinsch, N. Stock, *Chem. Commun.* **2016**, *52*, 12698–12701.
[24] S. Leubner, H. Zhao, N. Van Velthoven, M. Henrion, H. Reinsch, D. E. De Vos, U. Kolb, N. Stock, *Angew. Chem. Int. Ed.* **2019**, *58*, 10995–11000.
[25] S. Waitschat, H. Reinsch, M. Arpacioglu, N. Stock, *CrystEngComm* **2018**, *20*, 5108–5111.
[26] P. Ji, K. Manna, Z. Lin, X. Feng, A. Urban, Y. Song, W. Lin, *J. Am. Chem. Soc.* **2017**, *139*, 7004–7011.
[27] S. Leubner, V. E. G. Bengtsson, K. Synnatschke, J. Gosch, A. Koch, H. Reinsch, H. Xu, C. Backes, X. Zou, N. Stock, *J. Am. Chem. Soc.* **2020**, *142*, 15995–16000.
[28] S. Wang, L. Chen, M. Wahiduzzaman, A. Tissot, L. Zhou, I. A. Ibarra, A. Gutiérrez-Alejandre, J. S. Lee, J.-S. Chang, Z. Liu, J. Marrot, W. Shepard, G. Maurin, Q. Xu, C. Serre, *Matter* **2021**, *4*, 182–194.
[29] V. Guillerm, F. Ragon, M. Dan-Hardi, T. Devic, M. Vishnuvarthan, B. Campo, A. Vimont, G. Clet, Q. Yang, G. Maurin, G. Férey, A. Vittadini, S. Gross, C. Serre, *Angew. Chem. Int. Ed.* **2012**, *51*, 9267–9271.
[30] N. Stock, *Microporous Mesoporous Mater.* **2010**, *129*, 287–295.
[31] A. Coelho, TOPAS Academic, Coelho Software **2007**.
[32] Materials Studio, Accelrys Inc., San Diego **2009**.
[33] Zr–CAU-61: space group *C2/m*, $a = 21.1246(5)$ Å, $b = 14.7255(4)$ Å, $c = 7.8486(2)$ Å, $\beta = 87.028(2)°$, deposition number: 2258086; Hf–CAU-61: space group *C2/m*, $a = 21.0881(5)$ Å, $b = 14.6752(3)$ Å, $c = 7.81532(17)$ Å, $\beta = 87.0255(19)°$, deposition number: 2258085.
[34] R. C. Klet, Y. Liu, T. C. Wang, J. T. Hupp, O. K. Farha, *J. Mater. Chem. A* **2016**, *4*, 1479–1485.
[35] F. Ragon, B. Campo, Q. Yang, C. Martineau, A. D. Wiersum, A. Lago, V. Guillerm, C. Hemsley, J. F. Eubank, M. Vishnuvarthan, F. Taulelle, P.

Horcajada, A. Vimont, P. L. Llewellyn, M. Daturi, S. Devautour-Vinot, G. Maurin, C. Serre, T. Devic, G. Clet, *J. Mater. Chem. A* **2015**, *3*, 3294–3309.
[36] V. A. Blatov, A. P. Shevchenko, D. M. Proserpio, *Cryst. Growth Des.* **2014**, *14*, 3576–3586.
[37] Y. Zhao, D. G. Truhlar, *J. Phys. Chem. A* **2006**, *110*, 13126–13130.
[38] Č. Jovalekić, M. Zdujić, D. Poleti, L. Karanović, M. Mitrić, *J. Solid State Chem.* **2008**, *181*, 1321–1329.
[39] R. E. Hann, P. R. Suitch, J. L. Pentecost, *J. Am. Ceram. Soc.* **1985**, *68*, C-285–C-286.
[40] H. Motegi, K. Yano, N. Setoyama, Y. Matsuoka, T. Ohmura, A. Usuki, *J. Porous Mater.* **2017**, *24*, 1327–1333.
[41] A. H. Valekar, K.-H. Cho, S. K. Chitale, D.-Y. Hong, G.-Y. Cha, U.-H. Lee, D. W. Hwang, C. Serre, J.-S. Chang, Y. K. Hwang, *Green Chem.* **2016**, *18*, 4542–4552.
[42] S. Øien, D. Wragg, H. Reinsch, S. Svelle, S. Bordiga, C. Lamberti, K. P. Lillerud, *Cryst. Growth Des.* **2014**, *14*, 5370–5372.
[43] M. J. Kadhim, M. I. Gamaj, *J. Chem. Rev.* **2020**, *2*, 182–188.

Manuscript received: June 1, 2023
Accepted manuscript online: June 5, 2023
Version of record online: July 20, 2023